VIP Transient Oligomer Structures | Very Important Paper

DOI: 10.1002/ange.201402636

# Significant Structural Differences between Transient Amyloid-β Oligomers and Less-Toxic Fibrils in Regions Known To Harbor Familial Alzheimer's Mutations**

*Bidyut Sarkar, Venus Singh Mithu, Bappaditya Chandra, Arghya Mandal, Muralidharan Chandrakesan, Debanjan Bhowmik, Perunthiruthy K. Madhu,* and Sudipta Maiti**

***Abstract:*** *Small oligomers of the amyloid β (Aβ) peptide, rather than the monomers or the fibrils, are suspected to initiate Alzheimer's disease (AD). However, their low concentration and transient nature under physiological conditions have made structural investigations difficult. A method for addressing such problems has been developed by combining rapid fluorescence techniques with slower two-dimensional solid-state NMR methods. The smallest $A\beta_{40}$ oligomers that demonstrate a potential sign of toxicity, namely, an enhanced affinity for cell membranes, were thus probed. The two hydrophobic regions (residues 10–21 and 30–40) have already attained the conformation that is observed in the fibrils. However, the turn region (residues 22–29) and the N-terminal tail (residues 1–9) are strikingly different. Notably, ten of eleven known Aβ mutants that are linked to familial AD map to these two regions. Our results provide potential structural cues for AD therapeutics and also suggest a general method for determining transient protein structures.*

Early aggregates of amyloid β (Aβ) peptides are suspected to initiate Alzheimer's disease (AD).[1] As the monomers evolve to form ever larger aggregates, their structures and properties also change.[1d,2] As it is difficult to resolve the structure of a species that evolves on the timescale of minutes, the mechanism underlying Aβ oligomer toxicity remains poorly understood. Fluorescence-based techniques are fast and sensitive, but their structural resolution is poor. NMR spectroscopy can provide atomic-level structural resolution, but suffers from poor sensitivity and speed. Herein, we combine the power of these two techniques to study evolving Aβ oligomers. We observed structural differences between the toxic oligomers and the less toxic fibrils in specific regions of the peptide, which may provide clues towards the origin of Alzheimer's disease.

The structures of some of the transient Aβ oligomers have been probed by stabilizing these species under non-physiological conditions, for example, by using low temperatures,[3] low salt concentrations,[3–4] detergents,[5] antibodies,[6] or by grafting pieces of Aβ oligomer into crystallizable peptides.[7] In contrast, the structure of the less toxic[1b,8] fibrillar end state has been determined reasonably well by solid-state NMR (ssNMR) spectroscopy using fibrils that were grown in physiological solutions.[9] Notably, in a recent study, fibrils that were taken from post mortem AD brains were used as aggregation templates.[10]

The extent to which the structures of the stabilized oligomers resemble those formed under physiological conditions, or whether any of these structures constitute the initial toxic species, is not known. Recent fluorescence experiments suggested that the membrane affinity, a crucial parameter for the interaction of an extra-cellular peptide such as Aβ with cells, increases sharply in an early stage of aggregation.[11] These membrane-active $A\beta_{1-40}$ ($A\beta_{40}$) species appear to be small oligomers (*n*-mers with $n < 10$ and a hydrodynamic radius of ca. 1.5 nm).[11a,12] They have a closed conformation with the two termini in close proximity, a structural feature that makes them appear similar to the fibrils.[2] In contrast, the monomer is flexible with a large inter-terminal distance[2] and a partially alpha-helical structure.[13] This indicates that the acquisition of high membrane affinity is associated with a crucial structural transition, even though the details of this transition are not known.

An alternative approach to determine transient structures aside from stabilization in non-physiological conditions, is to freeze an evolving structure and perform multidimensional ssNMR experiments on the frozen or freeze-dried solid specimen.[3b] There are two problems in applying this strategy to the early $A\beta_{40}$ oligomers under physiological conditions: They evolve quickly (on a timescale of tens of minutes), and

[*] B. Sarkar,[+] Dr. V. S. Mithu,[+] B. Chandra,[+] A. Mandal, D. Bhowmik, Prof. P. K. Madhu, Prof. S. Maiti
Department of Chemical Sciences
Tata Institute of Fundamental Research
Homi Bhabha Road, Colaba, Mumbai 400005 (India)
E-mail: madhu@tifr.res.in
maiti@tifr.res.in
M. Chandrakesan
Department of Biochemistry
Seth G. S. Medical College and KEM Hospital
A. D. Marg, Parel, Mumbai 400012 (India)
Prof. P. K. Madhu
TIFR Centre for Interdisciplinary Sciences
21 Brundavan Colony, Narsinghi, Hyderabad 500075 (India)

[+] These authors contributed equally to this work.

[**] This work was supported by the SERC scheme of the Department of Science and Technology, India (P.K.M., SR/S1/PC/27/2009) and by the Dept. of Biotechnology, India (S.M., BT/53/NE/TBP/2010). We acknowledge the National Facility for High-Field NMR and the Cryo-TEM facilities, TIFR, and Manoj Naik, G. Krishnamoorthy and Mamata Kombrabail, and Lalit Borde for NMR, TCSPC, and TEM measurements, respectively.

Supporting information for this article is available on the WWW under http://dx.doi.org/10.1002/anie.201402636.

  

they are present at concentrations in the μM range (higher concentrations lead to increasingly faster aggregation). We therefore require a fast readout of the oligomer size and conformation and a method for separating small amounts of protein from the large amounts of salt and solvent that are present in a physiological buffer solution after freezing.

As we have recently shown, the first problem can be solved by using fast fluorescence techniques, that is, fluorescence correlation spectroscopy (FCS, which measures size) and Förster resonance energy transfer (FRET, which monitors conformation).[2] To address the second problem, we used a volatile buffer, which allowed us to remove both the solvent and the salt while keeping the protein intact in the frozen state. This procedure is presented in Figure 1 A. We continuously monitored an $A\beta_{40}$ solution (25 μM) with FCS

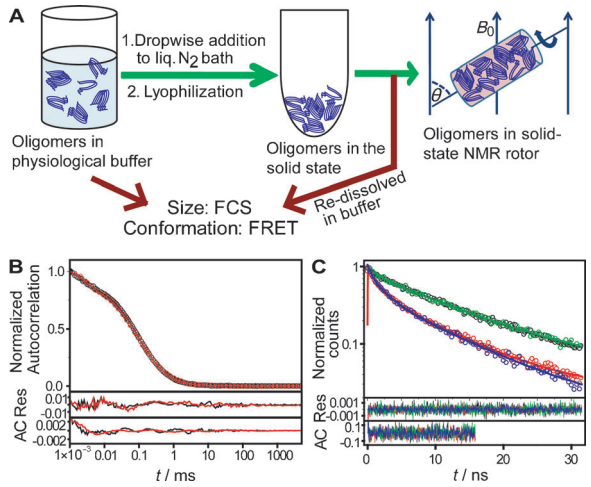


***Figure 1.*** A) Preparation of $A\beta_{40}$ oligomers for solid-state NMR spectroscopy and control experiments. B) Size (before lyophilization: black, after redissolution: red) determined by a single-component fit (——) to fluorescence autocorrelation data (○) of $A\beta_{40}$ labeled with rhodamine. C) The conformation of the $A\beta_{40}$ oligomers was determined by fitting time-correlated single photon counting (TCSPC) lifetime data (○) that was obtained from donor-labeled $A\beta_{40}$ (before: black, after: green) and donor–acceptor-labeled $A\beta_{40}$ (before: red, after: blue) to multi-exponential decay models (——). The fit residuals (Res) and the autocorrelation of the residuals (AC) are shown in the corresponding colors.

and FRET, after the solution had initially been prepared by diluting a stock solution with a high pH value with a volatile ammonium acetate buffer (with a physiological pH value of 7.4 and salt concentrations of 175 mM) at room temperature. When the species in the solution are typically able to bind to cell membranes (approximately 15–30 minutes after preparation),[11a] the solution was flash-freezed by adding solution droplets to liquid nitrogen. The mixture was lyophilized in the frozen state until the water and the volatile buffer had evaporated. The volatile buffer ensures that approximately 10–15 mg of the protein can be recovered from several hundred milliliters of dilute solution. This powder was then subjected to magic-angle spinning (MAS) ssNMR spectroscopy.

We first investigated whether this method of freeze-drying in a volatile buffer leaves the aggregate size and the peptide conformation unchanged. Small amounts of separate samples (25 μM $A\beta_{40}$) that contain rhodamine labeled $A\beta_{40}$ ($RA\beta_{40}$, 50 nM, for FCS measurements) or donor- or donor–acceptor-labeled $A\beta_{40}$ ($A\beta_{40}$-EDANS and Dabcyl-$A\beta_{40}$-EDANS, at a labeled/unlabeled peptide ratio of 1:5, for FRET studies) were subjected to the treatment described above. The FCS measurements before lyophilization (Figure 1 B; black line) yielded a diffusion time of $94.0 \pm 1.2$ μs in our home-built FCS instrument[14] (implying a hydrodynamic radius of $1.69 \pm 0.05$ nm). The FCS curve remained nearly unchanged for the redissolved lyophilized powder (Figure 1 B; red line), which yielded a hydrodynamic radius of $1.65 \pm 0.16$ nm. The FRET measurement before lyophilization (Figure 1 C; donor-labeled protein: black, donor–acceptor-labeled protein: red) revealed an inter-terminal distance of $2.0 \pm 0.2$ nm, whereas the FRET measurement after lyophilization (Figure 1 C; donor-labeled protein: green, donor–acceptor-labeled protein: blue) gave a distance of $2.1 \pm 0.3$ nm (see the Supporting Information for details). Therefore, our measurements have established that the lyophilization procedure leaves the size and the conformation of the oligomers unchanged, within experimental errors.

We also confirmed that the ammonium acetate buffer does not change the conformation of the protein, at least in the fibrils. We established the similarity with structures observed in more commonly used buffers (such as phosphate or HEPES buffered saline solutions),[9b,d–f] using transmission electron microscopy (TEM; Figure S1) and ssNMR spectroscopy (Figure S2).

We then compared the structure of the oligomers with that of the fibrils (both grown in ammonium acetate buffer) per region, using $^{13}C$–$^{13}C$ 2D correlation spectroscopy (Figure 2 A–C; blue: oligomer, red: fibril). We prepared three different isotopically labeled ($^{13}C$ and $^{15}N$) specimens, $S^1$, $S^2$, and $S^3$. $S^1$ was labeled at E11, F19, A30, L34, V36, and G38, $S^2$ at A2, V12, F20, D23, S26, K28, and M35, and $S^3$ at R5, D7, K16, A21, G25, N27, I32, and V40. All of the isotopically labeled residues are marked with black circles (Figure 3 A). The peak markers in Figure 2 A–C obey the region-wise color scheme that is depicted in Figure 3 A. We first considered the regions that constitute the mostly hydrophobic β-sheet arms in the structural models of the fibrils (residues 10–21 and 30–40, the region shaded green in Figure 3 A[9d]). There are 13 isotopically enriched residues in these two arm regions, at positions E11, V12, K16, F19, F20, A21, A30, I32, L34, M35, V36, G38, and V40. The $^{13}C$–$^{13}C$ correlation spectra show that the conformations for this region are remarkably similar for the oligomers and the fibrils (Figure 2 A–C; cross-peaks indicated by green lines; see Table S1 for the respective chemical-shift values). The secondary chemical-shift values ($\Delta\delta = \delta_{observed} - \delta_{random\ coil}$)[15] are shown in Figure 3 B (top panel; □: carbonyl carbon atoms, ○: α carbon atoms, △: β carbon atoms; blue: oligomers, red: fibrils). The chemical-shift differences between the two species ($\delta_{oligomers} - \delta_{fibrils}$) are also given in Figure 3 B (bottom panel; the yellow region corresponds to values of $> \pm 1$ ppm, which are considered to be very significant). Conformations with significant popula-

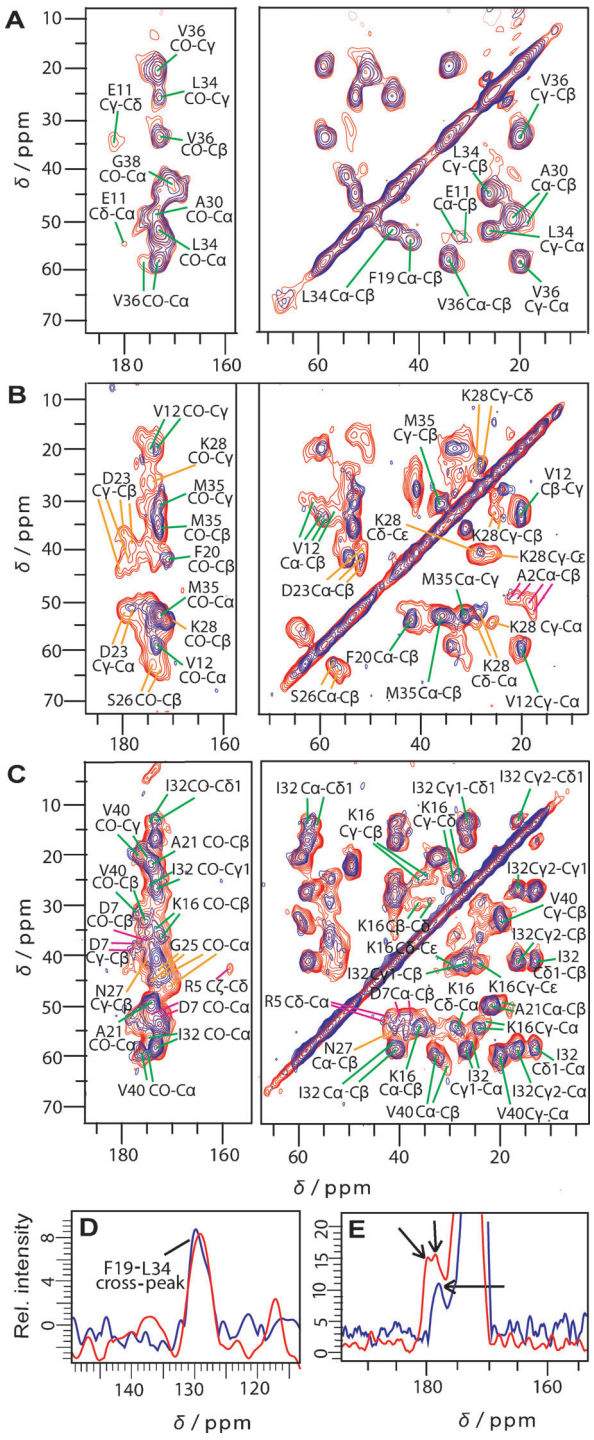


***Figure 2.*** A–C) Carbonyl (left panel) and aliphatic (right panel) regions of the $^{13}C$–$^{13}C$ 2D correlation spectra for $A\beta_{40}$ oligomers (blue) and fibrils (red) prepared in ammonium acetate buffer. Different amino acids are uniformly labeled with $^{13}C$ and $^{15}N$ to give three different $A\beta_{40}$ peptides: $S^1$ (A), $S^2$ (B), and $S^3$ (C). The colors of the peak markers correspond to the different parts of the peptide; magenta: residues 1–9; green: residues 10–21 and 30–40; orange: residues 22–29. D) 1D $^{13}C$ NMR spectra extracted from the 2D $^{13}C$–$^{13}C$ spectra of $S^1$ oligomers (blue) and fibrils (red) at 24.7 ppm. The cross-peak between the γ carbon atom of L34 and the aromatic (δ/ε/ζ) carbon atoms of F19 is indicated. E) Carbonyl region of the 1D sum projection (rows between 34.8–54.9 ppm) of 2D $^{13}C$–$^{13}C$ spectra of $S^2$ oligomers (blue) and fibrils (red). Different conformations yielded by the γ carbon atom of Asp23 are indicated by arrows.

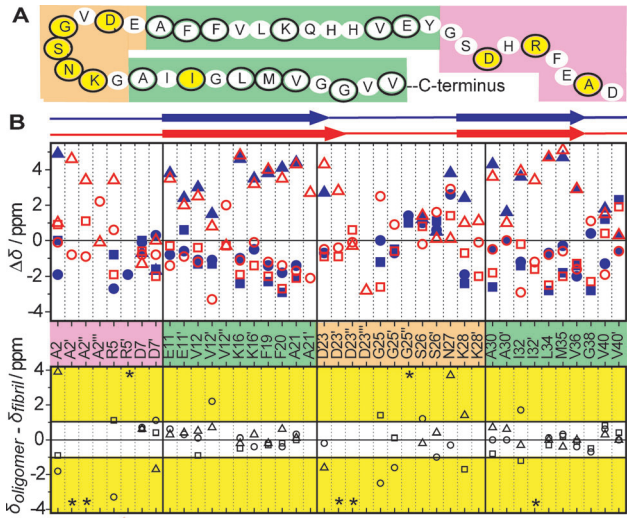


***Figure 3.*** A) Schematic representation of the $A\beta_{40}$ peptide (The color scheme is the same as for the peak markers in Figure 2A–C). $^{13}C$ and $^{15}N$ labeled residues are circled in black. Yellow circles denote residues with large chemical-shift differences ($\geq \pm 1.0$ ppm) between the oligomer and the fibril. B) Top panel: secondary chemical-shift plot for the α carbon atoms (○), β carbon atoms (△), and carbonyl carbon atoms (□) of all of the structural conformers of $A\beta_{40}$ oligomers (blue) and fibrils (red). Predicted β-sheet (thick arrows) and random coil (thin lines) regions are shown above the plot. Different residues of the $A\beta_{40}$ oligomers are highlighted as in (A). Bottom panel: chemical-shift differences of the major conformations of oligomers and fibrils ($\delta_{oligomers} - \delta_{fibrils}$). Yellow regions correspond to differences that are larger than 1.0 ppm (considered as strongly significant). All symbols have the same meaning as in the top panel. Conformations with significant populations that are observed for only one of the species (either oligomer or fibril) are marked with asterisks (*).

tions that were observed for only one of the species (either oligomer or fibril) are marked with asterisks (*). Secondary chemical-shift values strongly indicate that almost all of these residues adopt β-sheet conformations in both the oligomers and the fibrils (Figure 3B). Some of the residues yielded multiple sets of cross-peaks, which indicates structural polymorphism. This is a commonly observed phenomenon in amyloid systems.[9a,d] In each case, the major conformation is the same for the oligomers and the fibrils (Figure 3B, bottom panel). The only exception is I32, whose single conformation in the oligomer corresponds to the minor conformation in the fibril (I32′). Even the cross-peak between F19 and L34, which corresponds to a significant non-local interaction that is found in almost all fibrillar conformations studied thus far[9d–f,10,16] as well in protofibrils,[6] is observed for the oligomer. The unambiguous cross-peak between the γ carbon atom of L34 and the aromatic (δ/ε/ζ) carbon atoms of F19 is shown in an overlay of 1D slices that were extracted from the 2D $^{13}C$–$^{13}C$ phase-alternated recoupling irradiation scheme (PARIS-xy; $m = 1$, $N = 2$, mixing time = 400 ms)[17] spectra at 24.7 ppm (blue: oligomer, red: fibril; Figure 2D). The strong similarity of the structures in these two regions of the peptide chain has several implications. It suggests that a hydrophobic collapse of this region, accompanied by the formation of the final secondary structure, is the major initial event of fibril formation. Furthermore, the similarity also

suggests that these oligomers are "on-pathway" intermediates for fibril formation. Our data do not show any alpha-helical intermediates on the pathway to fibril formation, which have been reported in some studies.[18] These results also imply that this predominant early structural feature should be an important target for the design of an effective pharmaceutical reagent to disrupt the aggregation process. Our study explains several observations that revealed that reagents that disrupt fibril formation interact with these two regions.[8]

However, the fibrils are thought to be less toxic,[1b,8] and consequently one would expect the peptide conformation (and/or the inter-peptide packing, which was not probed in this study) to be significantly different between the fibrils and the oligomers. Conformational differences are indeed pronounced in the remaining regions of the peptide. We next examined the turn region (residues 22–29, shaded orange in Figure 3A, cross-peaks marked as before, labeled at positions D23, G25, S26, N27, and K28). The prominent feature of this region is the intermolecular salt bridge between D23 and K28 in the fibrils.[9c] This is also observed for the fibrils that were obtained by incubation of in vivo seeds from AD patients.[10] We also observed this salt bridge in fibrils grown in HEPES buffer (confirmed by an fsREDOR experiment, data not shown). The major peaks for the fibrils that were grown in ammonium acetate buffer have nearly identical chemical-shift values (Figure S2 and Table S1). However, these two residues have significantly different conformations in the oligomers. This is manifested in the chemical shifts of the side-chain carbonyl carbon atom of D23 (Figure 2B, left panel; $C_\gamma$–$C_\beta$ and $C_\gamma$–$C_\alpha$ cross-peaks indicated with orange arrows; see also Table S1). The difference is also clearly evident in the 1D sum projection of rows between 34.8–54.9 ppm of the 2D $^{13}C$–$^{13}C$ PARIS-xy spectra ($m = 1$, $N = 0.5$, mixing time = 100 ms) for $A\beta_{40}$ oligomers (Figure 2E; blue) and fibrils (Figure 2E; red). The peaks that are ascribed to different conformations of the Asp23 γ carbon atom are indicated by the arrows in Figure 2E. Correspondingly, the intra-residue cross-peaks of K28 are also very different for the fibril and the oligomer (Figure 2B). These findings may suggest, but do not confirm, the absence of the salt bridge. However, recent theoretical studies suggest that the salt bridge is present in the small oligomers.[19] The other residues in this region also show very different cross-peaks (Figure 2B,C, and highlighted in the yellow region of Figure 3B) with weaker peak intensities (except for G25) and multiple conformations. These peaks imply that this part of the oligomer is in an intermediate structural state and yet to take up the conformations that are observed in the protofibrils or fibrils.

Another region that shows major differences between the oligomers and the fibrils is the N-terminal tail (residues 1–9, highlighted in magenta in Figure 3A). This region is less structured in the fibrils than in the hydrophobic arm regions,[9a–d] although clear intra-residue cross-peaks are still observed (Figure 2B,C, magenta arrows). In fact, the order parameters for the N-terminal residues (which provide a measure of structural rigidity) are as high in the protofibrils as in the fibrils.[6] In contrast, in the oligomer spectrum, the cross-peaks observed for the labeled residues (A2, R5, and D7) are very weak. This implies that this region is more flexible in the oligomers than in the fibrils. The region-wise conformational differences are indicated in the yellow region of Figure 3B (bottom panel).

Therefore, we conclude that the turn region (Figure 3A, orange) and the N-terminal region (Figure 3A, magenta) are yet to acquire their final structures. Interestingly, ten of the eleven mutations in the Aβ protein that lead to familial Alzheimer's disease map to these two regions of the peptide (e.g., A2V, H6R English, D7N Tottori, D7H Taiwanese, and A21G Flemish, E22G Arctic, E22K Italian, E22Q Dutch, E22Δ Osaka, and D23N Iowa).[20] The mutation A2T, which also belongs to this region, is protective.[20] It is likely that single mutations can easily affect the structure and stability of the less structured regions, thereby strongly modifying their toxicity. Simulation studies have indeed suggested that N-terminal mutations can significantly alter the structural preferences of the peptide.[21] If the conformation of the early Aβ oligomers has a role to play in Alzheimer's disease, then the key to understanding this disease will possibly lie in the turn and the N-terminal regions of the peptide.

Received: February 21, 2014
Published online: April 24, 2014

**Keywords:** amyloid β-peptides · NMR spectroscopy · protein folding · toxic oligomers · transient structures

[1] a) C. A. McLean, R. A. Cherny, F. W. Fraser, S. J. Fuller, M. J. Smith, K. Beyreuther, A. I. Bush, C. L. Masters, *Ann. Neurol.* **1999**, *46*, 860–866; b) D. M. Walsh, D. J. Selkoe, *J. Neurochem.* **2007**, *101*, 1172–1184; c) I. Benilova, E. Karran, B. De Strooper, *Nat. Neurosci.* **2012**, *15*, 349–357; d) K. Ono, M. M. Condron, D. B. Teplow, *Proc. Natl. Acad. Sci. USA* **2009**, *106*, 14745–14750.

[2] S. Nag, B. Sarkar, M. Chandrakesan, R. Abhyanakar, D. Bhowmik, M. Kombrabail, S. Dandekar, E. Lerner, E. Haas, S. Maiti, *Phys. Chem. Chem. Phys.* **2013**, *15*, 19129–19133.

[3] a) S. Chimon, Y. Ishii, *J. Am. Chem. Soc.* **2005**, *127*, 13472–13473; b) S. Chimon, M. A. Shaibat, C. R. Jones, D. C. Calero, B. Aizezi, Y. Ishii, *Nat. Struct. Mol. Biol.* **2007**, *14*, 1157–1164; c) M. Ahmed, J. Davis, D. Aucoin, T. Sato, S. Ahuja, S. Aimoto, J. I. Elliott, W. E. Van Nostrand, S. O. Smith, *Nat. Struct. Mol. Biol.* **2010**, *17*, 561–567; d) W. M. Tay, D. Huang, T. L. Rosenberry, A. K. Paravastu, *J. Mol. Biol.* **2013**, *425*, 2494–2508.

[4] J. C. Stroud, C. Liu, P. K. Teng, D. Eisenberg, *Proc. Natl. Acad. Sci. USA* **2012**, *109*, 7717–7722.

[5] L. Yu, R. Edalji, J. E. Harlan, T. F. Holzman, A. P. Lopez, B. Labkovsky, H. Hillen, S. Barghorn, U. Ebert, P. L. Richardson, L. Miesbauer, L. Solomon, D. Bartley, K. Walter, R. W. Johnson, P. J. Hajduk, E. T. Olejniczak, *Biochemistry* **2009**, *48*, 1870–1877.

[6] H. A. Scheidt, I. Morgado, S. Rothemund, D. Huster, M. Fandrich, *Angew. Chem.* **2011**, *123*, 2889–2892; *Angew. Chem. Int. Ed.* **2011**, *50*, 2837–2840.

[7] J. D. Pham, N. Chim, C. W. Goulding, J. S. Nowick, *J. Am. Chem. Soc.* **2013**, *135*, 12460–12467.

[8] J. Bieschke, M. Herbst, T. Wiglenda, R. P. Friedrich, A. Boeddrich, F. Schiele, D. Kleckers, J. M. Lopez del Amo, B. A. Gruning, Q. Wang, M. R. Schmidt, R. Lurz, R. Anwyl, S. Schnoegl, M. Fandrich, R. F. Frank, B. Reif, S. Gunther, D. M. Walsh, E. E. Wanker, *Nat. Chem. Biol.* **2012**, *8*, 93–101.

[9] a) A. T. Petkova, R. D. Leapman, Z. Guo, W. M. Yau, M. P. Mattson, R. Tycko, *Science* **2005**, *307*, 262–265; b) T. Luhrs, C.

  

Ritter, M. Adrian, D. Riek-Loher, B. Bohrmann, H. Dobeli, D. Schubert, R. Riek, *Proc. Natl. Acad. Sci. USA* **2005**, *102*, 17342 – 17347; c) A. T. Petkova, W. M. Yau, R. Tycko, *Biochemistry* **2006**, *45*, 498 – 512; d) A. K. Paravastu, R. D. Leapman, W. M. Yau, R. Tycko, *Proc. Natl. Acad. Sci. USA* **2008**, *105*, 18349 – 18354; e) I. Bertini, L. Gonnelli, C. Luchinat, J. Mao, A. Nesi, *J. Am. Chem. Soc.* **2011**, *133*, 16013 – 16022; f) V. S. Mithu, B. Sarkar, D. Bhowmik, M. Chandrakesan, S. Maiti, P. K. Madhu, *Biophys. J.* **2011**, *101*, 2825 – 2832.

[10] J. X. Lu, W. Qiang, W. M. Yau, C. D. Schwieters, S. C. Meredith, R. Tycko, *Cell* **2013**, *154*, 1257 – 1268.

[11] a) B. Sarkar, A. K. Das, S. Maiti, *Front. Physiol.* **2013**, *4*, 84; b) P. Narayan, K. A. Ganzinger, J. McColl, L. Weimann, S. Meehan, S. Qamar, J. A. Carver, M. R. Wilson, P. St George-Hyslop, C. M. Dobson, D. Klenerman, *J. Am. Chem. Soc.* **2013**, *135*, 1491 – 1498.

[12] S. Nag, B. Sarkar, A. Bandyopadhyay, B. Sahoo, V. K. Sreenivasan, M. Kombrabail, C. Muralidharan, S. Maiti, *J. Biol. Chem.* **2011**, *286*, 13827 – 13833.

[13] a) D. Bhowmik, C. M. Maclaughlin, M. Chandrakesan, P. Ramesh, R. Venkatramani, G. C. Walker, S. Maiti, *Phys. Chem. Chem. Phys.* **2014**, *16,* 885 – 889; b) I. H. Chou, M. Benford, H. T. Beier, G. L. Cote, M. Wang, N. Jing, J. Kameoka, T. A. Good, *Nano Lett.* **2008**, *8*, 1729 – 1735.

[14] P. Sengupta, J. Balaji, S. Maiti, *Methods* **2002**, *27*, 374 – 387.

[15] D. S. Wishart, C. G. Bigam, A. Holm, R. S. Hodges, B. D. Sykes, *J. Biomol. NMR* **1995**, *5*, 67 – 81.

[16] M. Chandrakesan, B. Sarkar, V. S. Mithu, R. Abhyankar, D. Bhowmik, S. Nag, B. Sahoo, R. Shah, S. Gurav, R. Banerjee, S. Dandekar, J. C. Jose, N. Sengupta, P. K. Madhu, S. Maiti, *Chem. Phys.* **2013**, *422*, 80 – 87.

[17] M. Weingarth, D. E. Demco, G. Bodenhausen, P. Tekely, *Chem. Phys. Lett.* **2009**, *469*, 342 – 348.

[18] M. D. Kirkitadze, M. M. Condron, D. B. Teplow, *J. Mol. Biol.* **2001**, *312*, 1103 – 1119.

[19] M. H. Viet, P. H. Nguyen, S. T. Ngo, M. S. Li, P. Derreumaux, *ACS Chem. Neurosci.* **2013**, *4*, 1446 – 1457.

[20] M. Cruts, J. Theuns, C. Van Broeckhoven, *Hum. Mutat.* **2012**, *33*, 1340 – 1344.

[21] P. H. Nguyen, B. Tarus, P. Derreumaux, *J. Phys. Chem. B* **2014**, *118*, 501 – 510.